Dynamic shear damage with frictional sliding on microcracks

Megbeme K Atiezo, Kokouvi Gbetchi, Cristian Dascalu

Dynamic shear damage with frictional sliding on microcracks

Megbeme K. Atiezo, Kokouvi Gbetchi, Cristian Dascalu

Université de Lorraine, CNRS, Arts et Métiers ParisTech, LEM3, F-57000 Metz, France

Abstract

A new damage model for rapid shear failure in brittle solids is constructed in the present contribution using a two-scale approach. The model is obtained by asymptotic homogenization from microstructures with dynamically evolving microcracks, in mode II, with unilateral contact and friction conditions on their lips. The analysis of the local effective response of the model reveals strain-rate and microstructural size effects and the influence of the small-scale friction. Results of numerical simulations for mode II brittle failure of PMMA specimens under impact loading are presented and compared with the experimental data. The failure evolution is found to be in good agreement with that reported in the experiments.

Keywords: microcracks, mode II dynamic propagation, contact and friction, asymptotic homogenization, damage law, shear failure, impact test.

Nomenclature

$\mathbf{u}$	displacement vector	ρ	mass density
$\boldsymbol{\sigma}$	stress tensor	$\mathbf{e}$	strain tensor
λ, μ	Lamé constants	a_{ijkl}	elastic coefficients
$\mathcal{G}$	energy-release rate	U	elastic energy
T	kinetic energy	$\mathbf{N}$, $\mathbf{T}$	normal, tangent unit vectors
ε	microstructural length	l	microcrack length
d	damage variable	Y	damage energy-release rate
$\Sigma_{ij}^{(0)}$	macroscopic stress tensor	C_{ijmn}	effective coefficients
c_R	Rayleigh wave velocity	μ_f	friction coefficient
$\mathcal{G}_c$	critical fracture energy	Y_f	frictional dissipation energy
I_{ijkl}	effective dissipation coefficient	$\mathbf{x}$	macroscopic variables
$\mathbf{y}$	microscopic variables	B	unit cell
CB	crack line in the unit cell	E, ν	Young modulus, Poisson ratio

1. Introduction

Many complex mechanical behaviors of quasi-brittle materials under compression loadings, including the material hardening and softening, elastic stiffness degradation, induced anisotropy, irreversible deformations, have as microscopic origins the propagation of microcracks and the frictional sliding along their lips. A proper modeling of the overall behavior of quasi-brittle materials should necessarily account for the two microscopic dissipative mechanisms and their coupling. Such a description is particularly challenging in the context of dynamics, when the material response is sensitive to the

rate of the applied loadings and specific interactions between the small-scale fracture and friction processes take place.

Among the various studies in the literature, one can mention the micro-mechanical approaches for stationary or evolving frictional micro-cracks in Kachanov (1982), Leguillon and Sanchez-Palencia (1982), Andrieux et al. (1986), Ashby and Hallam (1986), Horii and Nemat-Nasser (1986), Nemat-Nasser and Obata (1988), Telega (2014), Lee and Ju (1991), Gambarotta and Lagomarsino (1993), Halm and Dragon (1998), Lawn and Marshall (1998), Zhu and Shao (2015), Zhu et al. (2016).

In the context of dynamics, several models based on micro-mechanics have been developed to study the compressive failure response of brittle solids in the case when the main microscopic mechanism is the tensile fracture mode. Nemat-Nasser and Deng (1994) studied an array of interacting and dynamically growing wing cracks and estimated the rate-dependent dynamic damage evolution. Ravichandran and Subhash (1995) developed a micro-mechanical model for ceramics based on non-interacting, uniformly distributed sliding micro-cracks subjected to dynamic compressive loading and predicted effects of the rate sensitivity on failure strength. Huang et al. (2002) developed a model that combined damage evolution theory with dynamic crack growth under uniaxial dynamic compression. Paliwal and Ramesh (2008) developed a model based on the evolution of tensile wing micro-cracks in the case of uniaxial compression under constant strain loading. A more recent dynamic damage model inspired by the same wing crack mechanism and valid over a wide range of loading rates has been proposed by Bhatt et al. (2012).

Probabilistic damage models for the description of the fragmentation pro-

cesses have been proposed by Denoual and Hild (2000), Forquin and Hild (2010) based on the hypothesis that the increment of microcrack density is a function of the obscuration probability due to the stress release around newly formed microcracks. A specific microplane model for impact comminution of solids, inspired by the Grady's model of fragmentation and considering the kinetic energy in high-rate shear deformations as the driving force of comminution, has been formulated in Bazant and Caner (2014).

Most of these models are essentially based on mode I fracture mechanisms. However, there are physical situations in which cracks are constrained to propagate in mode II. Rupture on geological faults that occurs in earthquakes is a classical example. Impact experiments of Rosakis et al. (1999, 2000); Ravi-Chandar et al. (2000); Bjerke (2002); Bjerke and Lambros (2003) on bonded or side-grooved samples of brittle polymers revealed that under high strain rate loadings a failure mode transition from opening to shear fracture takes place. In contrast with the mode I crack velocities that are much smaller than the theoretical limit, the Rayleigh wave speed c_R, the shear cracks may evolve rapidly up to c_R and may pass in the supershear regime, with tip velocities v larger than the shear wave speed c_S.

Fracture Mechanics studies on dynamic mode II cracks (Freund, 1979, 1998; Burridge et al., 1979; Broberg, 1989, 1995, 1999; Slepyan, 2002; Ravi-Chandar, 2004) showed the possibility of intersonic propagation $c_S < v < c_L$, with c_L the dilatational wave speed, while the subsonic super-Rayleigh regime $c_R < v < c_S$ is non-physical since as it corresponds to negative values of the energy-release rate. In the intersonic interval, non-vanishing positive energy fluxes at the crack tip are obtained if a finite size cohesive zone model is

adopted, indicating the necessity of a distributed approach. Using a phase-field fracture model Schlüter et al. (2016) simulated the intersonic shear fracture of brittle specimens under impact, by triggering the crack path with a weak strip of reduced toughness, and obtained crack velocities in agreement with the experimental values in Rosakis et al. (2000).

The microstructural observations of the fracture surfaces reported in Ravi-Chandar et al. (2000) and Archer and Lesser (2010), for mode II failure of PMMA samples under impact, revealed the existence of complex morphologies which do not correspond to *en echelon* mode I microcracks, but rather to a mode II process zone. It was also observed (Bjerke, 2002; Bjerke and Lambros, 2003) that frictional contact plays an important role during the shear failure, leading to temperature rise up to the glass transition temperature and polymer melting effects. In this context, the present contribution investigates the possibility of modeling the dynamic shear failure of brittle solids using a damage model obtained by upscaling of microstructures with rapidly evolving mode II frictional microcracks.

Damage models have been extensively employed in the last years (e.g. phase-field, delay damage laws...) for the modeling of failure in solids. A method to obtain damage evolution laws from microcracks propagation criteria, using the asymptotic homogenization technique, has been proposed in Dascalu et al. (2008) and extended to more complex microcrack evolutions in Dascalu et al. (2010a,b); François and Dascalu (2010); Markenscoff and Dascalu (2012); Dobrovat et al. (2015). In dynamics, a damage model has been established for mode I microcracks in Keita et al. (2014); Dascalu (2018) and for the antiplane mode in Atiezo and Dascalu (2017). Heat dissipation effects

have been included in the mode I dynamic damage approach in Dascalu and Gbetchi (2019). Wrzesniak et al. (2015) proposed a quasi-static damage law for the in-plane shear-mode propagation of frictional microcracks.

The main objective of the present work is to develop a two-scale damage model by asymptotic homogenization from microstructures with microcracks propagating dynamically in mode II and having contact and friction conditions on their lips. The local analysis of the macroscopic response will be performed in order to reveal the main features of the new approach. At the structural level, the mode II brittle failure of PMMA specimens under impact loading will be reproduced numerically in order to illustrate the prediction capacity of the model.

The paper is organized as follows. In section 2, the initial elasto-dynamic fracture problem is formulated. The next two sections are devoted to the homogenization analysis to construct the macroscopic elastodynamics equations for the microcracked solid and the dynamic damage law deduced from the microscopic propagation criterion. The analysis of the local macroscopic response of the new model is performed in Section 5 for the effective coefficients, the influence of small-scale friction, the strain-rate and microstructural size effects. Results of numerical simulations for dynamic shear rupture of PMMA samples under impact loading are presented and compared with the experimental data in Section 6.

2. Formulation of the initial fracture problem

We consider the dynamic evolution of an elastic solid containing a locally periodic distribution of microcracks, parallel to the x_1 axis, as illustrated

in Figure 1. It is assumed that the microcracks are straight and equally distanced with the mutual distance between their centers denoted by ε. The length ε, assumed to be the same everywhere in the solid domain, is also the dimension of the square period containing a centered microcrack. The length of microcracks is denoted by l and may vary in space and time. The local periodicity assumption means that in the vicinity of a macroscopic point the spatial variations of l are small enough such that, locally, the microstructure may be considered periodic. However, large-scale variations of the microcrack length are allowed.

The equations of elastodynamics can be written :

$$\frac{\partial \sigma_{ij}^{\varepsilon}}{\partial x_i} = \rho \frac{\partial^2 u_j^{\varepsilon}}{\partial t^2} \tag{1}$$

and the constitutive relations of linear elasticity are :

$$\sigma_{ij}^{\varepsilon} = a_{ijkl} e_{xkl}(\mathbf{u}^{\varepsilon}) \tag{2}$$

where $\mathbf{u}^{\varepsilon}$ et $\boldsymbol{\sigma}^{\varepsilon}$ are the displacement and stress fields, ρ the mass density and e_{xkl} is the linearized strain tensor :

$$e_{xkl}(\mathbf{u}^{\varepsilon}) = \frac{1}{2}\left(\frac{\partial u_k}{\partial x_l} + \frac{\partial u_l}{\partial x_k}\right) \tag{3}$$

relative to the x_i variables. The elastic coefficients a_{ijkl} for an isotropic homogeneous solid have for expression :

$$a_{ijkl} = \lambda \delta_{ij}\delta_{kl} + \mu(\delta_{ik}\delta_{jl} + \delta_{il}\delta_{jk}) \tag{4}$$

where λ and μ are the Lamé constants.

Unilateral contact conditions are assumed on the crack lips. They can be expressed by the relations :

$$[\boldsymbol{\sigma}^{\varepsilon}\mathbf{N}] = 0, \quad \mathbf{N}\boldsymbol{\sigma}^{\varepsilon}\mathbf{N} < 0, \quad [\mathbf{u}^{\varepsilon}.\mathbf{N}] = 0 \tag{5}$$

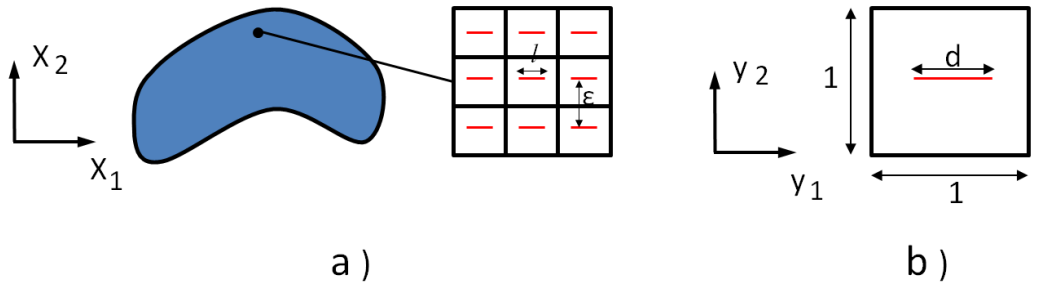

FIGURE 1: Micro-fissured medium with locally periodic microstructure : ε is the size of a period and l is the micro-crack length. b) Unit cell with rescaled crack of length $d = l/\varepsilon$.

where [.] represents the jump across the crack line with respect to the unit normal vector $\mathbf{N}$, oriented in the direction of the x_2 axis.

In addition to the contact relations (5), the Coulomb friction conditions are also considered such that, in the sliding regime, we have :

$$|\mathbf{T}\boldsymbol{\sigma}^{\varepsilon}\mathbf{N}| = -\mu_f \mathbf{N}\boldsymbol{\sigma}^{\varepsilon}\mathbf{N} \tag{6}$$

where $\mathbf{T}$ is the unit tangent vector to the crack, oriented in direction of x_1 axis, and μ_f is the friction coefficient.

We assume that microcracks are evolving symmetrically with respect to the center of the elementary period and following a Griffith-type propagation criterion based on the dynamic energy-release rate (Freund, 1998) :

$$\mathcal{G}^{d\varepsilon} = \lim_{r\to 0} \int_{\Gamma_r} \left((U+T)\mathbf{n}.\mathbf{e}_c - \sigma_{ij}^{\varepsilon} n_j \frac{\partial u_i^{\varepsilon}}{\partial x_1} \right) ds \tag{7}$$

where Γ_r is a circular contour of radius r surrounding the crack tip and $\mathbf{n}.\mathbf{e}_c$ is the scalar product of the outward unit normal $\mathbf{n}$ to Γ_r and the unit vector $\mathbf{e}_c$ having the same orientation as the velocity at the crack tip. The terms U

and T are, respectively, the elastic and the kinetic energy densities :

$$U = \frac{1}{2} a_{mnkl} e_{xkl}(u^\epsilon) e_{xmn}(u^\epsilon) \quad ; \quad T = \frac{1}{2} \rho \frac{\partial u^\varepsilon}{\partial t} \frac{\partial u^\varepsilon}{\partial t} \tag{8}$$

The propagation laws for microcracks are written in the form (e.g. Li et al., 2016) :

$$\dot{l} \geq 0; \qquad \mathcal{G}^{d\varepsilon} - \mathcal{G}_c \leq 0; \qquad \dot{l} \left(\mathcal{G}^{d\varepsilon} - \mathcal{G}_c \right) = 0 \tag{9}$$

where l is the microcrack length, $\mathcal{G}_c$ is the critical fracture energy of the material and $\dot{l}$ represents the time derivative of $l(t)$. The conditions (9) assure that the crack propagation is irreversible and it is allowed only when the available energy for fracture $\mathcal{G}^{d\varepsilon}$ reaches the critical energy $\mathcal{G}_c$ necessary to break the material bonds.

The objective of the next two sections is to construct a macroscopic elasto-damage model by homogenization of the present elastodynamic fracture problem.

3. Homogenized elastodynamic equations

In this section, we use the homogenization method based on asymptotic developments (Bakhvalov et al., 1989; Bensoussan et al., 1978; Sanchez-Palencia, 1980) to deduce the effective elastodynamic response of solids containing a large number of microcracks with contact and friction conditions. This section will extend the quasi-static analysis in Wrzesniak et al. (2015) to dynamics. The results will serve as a necessary basis for the construction of the damage model in the next section.

Two coordinate systems $\mathbf{x}$ and $\mathbf{y}$ are introduced for the homogenization method : the $\mathbf{x}$ variables are used to describe variations of the mechanical

fields at the macroscopic scale, while $\mathbf{y}$ variables refer to the microscopic scale. They are linked by the relation $\mathbf{y} = \frac{\mathbf{x}}{\varepsilon}$, where ε is the size of the period or the mutual distance between neighbor microcracks, as in Fig. 1. The above relation transforms the physical period of size ε, containing a crack of length l, in the unit cell B with a crack denoted BY of length $d = l/\varepsilon$.

The normalized crack length d will play the role of damage variable in our analysis. To understand the physical meaning of d, consider a damaged region of size L in the x_1 direction and suppose that $L = n.\varepsilon$. If the depth of the solid in the third dimension x_3 is denoted by D then, in a $x_1 - x_3$ section of area $L.D$, the total area of the microcracks is $n.l.D$. In this case, the damage variable $d = \frac{l}{\varepsilon} = \frac{n.l.D}{n.\varepsilon.D}$ represents the ratio of the area of microcracks over the total area of the section. Thus, we retrieve the classical definition of a damage variable. We also note that the local periodicity assumption for the length l allows for large-scale spatial variations of the damage variable d.

Following the asymptotic homogenization method, we consider the two-scale developments of the displacement and stress fields :

$$u_i^{\varepsilon}(\mathbf{x}, t) = u_i^{(0)}(\mathbf{x}, \mathbf{y}, t) + \varepsilon u_i^{(1)}(\mathbf{x}, \mathbf{y}, t) + \varepsilon^2 u_i^{(2)}(\mathbf{x}, \mathbf{y}, t) + \dots \tag{10}$$

$$\sigma_{ij}{}^{\varepsilon}(x, t) = \frac{1}{\varepsilon}\sigma_{ij}{}^{(-1)}(\mathbf{x}, \mathbf{y}, t) + \sigma_{ij}{}^{(0)}(\mathbf{x}, \mathbf{y}, t) + \varepsilon\sigma_{ij}{}^{(1)}(\mathbf{x}, \mathbf{y}, t) + ... \tag{11}$$

where $u_i^{(i)}(\mathbf{x}, \mathbf{y}, t)$ and $\sigma_{ij}^{(i)}(\mathbf{x}, \mathbf{y}, t)$ are periodic functions with respect to $\mathbf{y}$ in the unit cell B.

By replacing the expressions of u_i and σ_{ij} in the elastodynamic equations (1) and separating the terms of the same order in ε, we obtain a series of equations. The first three of them are :

$$\frac{\partial \sigma_{ij}^{(-1)}}{\partial y_i} = 0, \quad \frac{\partial \sigma_{ij}^{(-1)}}{\partial x_i} + \frac{\partial \sigma_{ij}^{(0)}}{\partial y_i} = 0, \quad \frac{\partial \sigma_{ij}^{(0)}}{\partial x_i} + \frac{\partial \sigma_{ij}^{(1)}}{\partial y_i} = \rho \frac{\partial^2 u_j^{(0)}}{\partial t^2} \tag{12}$$

In the same way, by replacing the two-scale developments in the constitutive relations (2), we obtain at the first orders in ε :

$$\sigma_{ij}^{(-1)} = a_{ijkl} e_{ykl}(\mathbf{u}^{(0)}) \tag{13}$$

$$\sigma_{ij}^{(0)} = a_{ijkl}(e_{xkl}(\mathbf{u}^{(0)}) + e_{ykl}(\mathbf{u}^{(1)})) \tag{14}$$

$$\sigma_{ij}^{(1)} = a_{ijkl}(e_{xkl}(\mathbf{u}^{(1)}) + e_{ykl}(\mathbf{u}^{(2)})) \tag{15}$$

Concerning the boundary conditions on the faces of the cracks, in the frictional sliding regime, we find at powers $m = -1, 0, \ldots$ of ε :

$$\left[\sigma_{ij}^{(m)} N_j\right] = 0, \;\; N_i {\sigma_{ij}}^{(m)} N_j < 0, \;\; |T_i \sigma_{ij}^{(m)} N_j| = -\mu_f N_i {\sigma_{ij}}^{(m)} N_j \text{ on } CB \tag{16}$$

together with the continuity of normal displacements :

$$\left[\mathbf{u}^{(p)}.\mathbf{N}\right] = 0, \quad \text{on} \quad CB \tag{17}$$

for p=0,1... The conditions (16 - 17) are formulated on the lips of the crack CB in the unit cell B. They are derived from the frictional contact conditions (5 - 6) through the transformation $\mathbf{y} = \frac{\mathbf{x}}{\varepsilon}$ and separating the terms of different orders in the asymptotic developments.

When the expression (13) is used in the first equation (12) and in the relations (16), for m=-1, we get the unit cell problem for $\mathbf{u}^{(0)}$:

$$\frac{\partial}{\partial y_i}(a_{ijkl} e_{ykl}(\mathbf{u}^{(0)})) = 0 \quad \text{in} \quad B \tag{18}$$

$$\left[(a_{ijkl} e_{ykl}(\mathbf{u}^{(0)}))N_j\right] = 0 \text{ on } CB \tag{19}$$

$$N_i(a_{ijkl} e_{ykl}(\mathbf{u}^{(0)}))N_j < 0 \text{ on } CB \tag{20}$$

$$|T_i(a_{ijkl} e_{ykl}(\mathbf{u}^{(0)}))N_j| = -\mu_f N_i(a_{ijkl} e_{ykl}(\mathbf{u}^{(0)}))N_j \text{ on } CB \tag{21}$$

with periodic boundary conditions on the opposite edges of the cell. This allows us to deduce the solution $\mathbf{u}^{(0)} = \mathbf{u}^{(0)}(\mathbf{x}, t)$ not depending on the microscopic variable $\mathbf{y}$ and thus becoming the macroscopic displacement field.

The problem for $\mathbf{u}^{(1)}$ is obtained by replacing the equation (14) in the second relation of (12) and in the relations (16), for m=0 :

$$\frac{\partial}{\partial y_i}(a_{ijkl}e_{ykl}(\mathbf{u}^{(1)})) = 0 \quad \text{in} \quad B \tag{22}$$

$$\left[(a_{ijkl}e_{ykl}(\mathbf{u}^{(1)}))N_j\right] = -\left[(a_{ijkl}e_{xkl}(\mathbf{u}^{(0)}))N_j\right] \text{ on } CB \tag{23}$$

$$N_i a_{ijkl}(e_{ykl}(\mathbf{u}^{(1)}) + e_{xkl}(\mathbf{u}^{(0)}))N_j < 0 \text{ on } CB \tag{24}$$

$$|T_i a_{ijkl}(e_{ykl}(\mathbf{u}^{(1)})+e_{xkl}(\mathbf{u}^{(0)}))N_j| = -\mu_f N_i a_{ijkl}(e_{ykl}(\mathbf{u}^{(1)})+e_{xkl}(\mathbf{u}^{(0)}))N_j \text{ on } CB \tag{25}$$

By introducing the macroscopic stress as the average value over the unit cell B :

$$\Sigma_{ij}^{(0)} \equiv \left\langle \sigma_{ij}^{(0)} \right\rangle = \frac{1}{|B|}\int_B a_{ijkl}(e_{xkl}(\mathbf{u}^{(0)}) + e_{ykl}(\mathbf{u}^{(1)}))dy \tag{26}$$

the homogenized macroscopic equation is obtained as :

$$\frac{\partial}{\partial x_j}\Sigma_{ij}^{(0)} = \rho\frac{\partial^2 u_i^{(0)}}{\partial t^2} \tag{27}$$

As proved in the Appendix, the stress expression (26) can be used to obtain the macroscopic constitutive relation :

$$\Sigma_{ij}^{(0)} = C_{ijmn}e_{xmn}(\mathbf{u}^{(0)}) \tag{28}$$

where the effective coefficients C_{ijmn} are given by the relations (56 - 58). We note that these coefficients depend on the normalized crack length d. This dependence will be illustrated numerically in Section 5.

4. Dynamic damage law with friction effects

In this section, the asymptotic homogenization method is used in combination with an energy analysis for microcracks propagating dynamically, in mode II, with contact and friction conditions, in order to obtain a macroscopic damage law.

The effective coefficients (56-58) depend on the damage variable d. Under the applied loadings, the microcracks are propagating and the variable $d(\mathbf{x}, t)$ will evolve in time at every material point $\mathbf{x}$. In order to describe this evolution, a macroscopic damage law is necessary. A specific upscaling procedure, from microcracks to damage, has been proposed in previous studies (Dascalu et al., 2008; François and Dascalu, 2010; Wrzesniak et al., 2015; Keita et al., 2014) and the objective of this section is to extend this approach to the case of dynamically propagating microcracks in contact with friction.

By replacing the asymptotic expansions of the displacement $\mathbf{u}^\epsilon$ and the stress $\boldsymbol{\sigma}^\varepsilon$ in (7) and taking into account the singularity of the mechanical fields, we obtain the expression of $\mathcal{G}^{d\varepsilon}$ in the form :

$$\mathcal{G}^{d\varepsilon} = \epsilon \lim_{r\to 0} \int_{\Gamma B_r} (-a_{ijkl} e_{ykl}(\mathbf{u}^{(1)}) n_j (\frac{\partial u_i^{(1)}}{\partial y_1}) + \frac{1}{2} a_{mnkl} e_{ykl}(\mathbf{u}^{(1)}) e_{ymn}(\mathbf{u}^{(1)}) + \frac{1}{2} \rho v^2 (\frac{\partial \mathbf{u}^{(1)}}{\partial y_1})^2) \, n_1 ds_y \tag{29}$$

where the change of variable $dS = \epsilon ds_y$ has been made, ΓB_r is the image of Γ_r in the unit cell B and the microcrack tip speed has been written $v = \epsilon \frac{\dot{d}}{2}$ together with the near-tip asymptotic relation (Freund, 1998) $\frac{\partial \mathbf{u}^\varepsilon}{\partial t} \simeq -v \frac{\partial \mathbf{u}^\varepsilon}{\partial x_1}$.

The dynamic energy-release rate can be expressed (Freund, 1998; Slepyan, 2002) as :

$$\mathcal{G}^{d\varepsilon} = g_2(v) \mathcal{G}^\varepsilon \tag{30}$$

where $\mathcal{G}^{\varepsilon}$ is the quasi-static energy-release rate, corresponding to (29) without the kinetic energy term, and g_2 is a universal function, for the mode II propagation, given by the formula :

$$g_2(v) = -\sqrt{\frac{1+\frac{v}{c_2}}{1-\frac{v}{c_2}}}\frac{v^2(1-\frac{v}{c_R})^2}{(1-\nu)c_2^2 R(v)D_+^2(v)} \tag{31}$$

Here $c_2 = \sqrt{\frac{\mu}{\rho}}$, $c_1 = \sqrt{\frac{E(1-\nu)}{\rho(1+\nu)(1-2\nu)}}$ are respectively the shear and dilatational wave velocities, c_R is the Rayleigh wave velocity. $R(v)$ and $D_+(v)$ are functions of crack velocity v given by the expressions (Slepyan, 2002) :

$$R(v) = (1+m_2^2)^2 - 4m_1m_2 \tag{32}$$

$$D_+(v) = exp(\frac{1}{\pi}\int_{c2/c1}^{1}\frac{\phi(\alpha)}{\alpha - c_2/v}d\alpha) \tag{33}$$

with

$$\phi(\alpha) = \arctan\frac{4\alpha^2\sqrt{1-\alpha^2}\sqrt{\alpha^2 - c_2/c_1}}{(2\alpha^2-1)^2} \tag{34}$$

and the constants $m_{1,2} = \sqrt{1-\frac{v^2}{c_{1,2}^2}}$.

In order to find a dynamic damage law in a relatively simple form, we seek for an explicit approximation of the function $g_2(v)$. Using numerical integration for $D_+(v)$, we can compute $g_2(v)$ for v ranging from 0 to c_R. Its graphical representation is given in Figure 2 and compared to other simple approximation functions $g_2(v) \approx g_2^{\alpha}(v)$ of the form

$$g_2^{\alpha}(v) = \sqrt{1-(\frac{v}{c_R})^{\alpha}} \tag{35}$$

We remark that reasonably good approximations are obtained for $\alpha = 0.9$ and $\alpha = 1$.

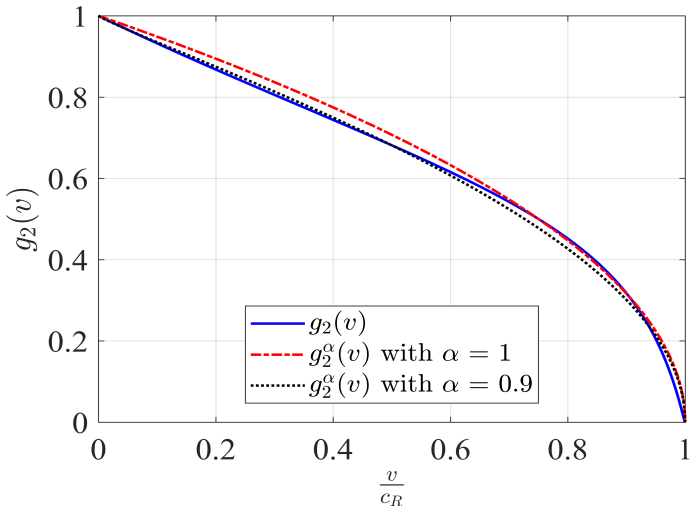

FIGURE 2: The function $g_2(v)$ and its approximations $g_2^\alpha(v)$ for $\alpha = 1$ and $\alpha = 0.9$.

Since the unit cell problem given in the previous section is the same as in quasi-statics, the analysis performed in Wrzesniak et al. (2015) is still valid. In particular, it allows to obtain a quasi-static damage relation :

$$\left(\frac{\mathcal{G}^\varepsilon}{\varepsilon} + (\frac{1}{2}\frac{\partial C_{mnpq}}{\partial d} + I_{mnpq}) e_{xmn}(\mathbf{u}^{(0)}) e_{xpq}(\mathbf{u}^{(0)}) \right) \dot{d} = 0 \tag{36}$$

where the effective integral terms I_{mnpq} are described in the Appendix. The corresponding terms in the laws (59) and (36) are related to the energy dissipated by friction on the lips of microcracks. They are absent in the case of frictionless contact or opening crack face conditions.

The term $\mathcal{G}^\varepsilon$ in (36) can be expressed as $\mathcal{G}^\varepsilon = \mathcal{G}^{d\varepsilon}/g_2(v)$ from (30). And using the Griffith propagation criterion $\mathcal{G}^{d\varepsilon} = \mathcal{G}_c$ for $\dot{d} \neq 0$, we get the damage evolution law :

$$\dot{d} = \frac{2c_R}{\varepsilon} \left\langle 1 - \frac{\mathcal{G}_c^2}{(\varepsilon(\frac{1}{2}\frac{\partial C_{mnpq}}{\partial d} + I_{mnpq}) e_{xmn}(\mathbf{u}^{(0)}) e_{xpq}(\mathbf{u}^{(0)}))^2} \right\rangle^{1/\alpha} \tag{37}$$

where $\langle . \rangle$ represents the positive part. If we introduce the notation $Y_f = I_{mnpq} e_{xmn}(\mathbf{u}^{(0)}) e_{xpq}(\mathbf{u}^{(0)})$ for the frictional dissipation term and the damage energy-release rate $Y = -\frac{1}{2}\frac{\partial C_{mnpq}}{\partial d} e_{xmn}(\mathbf{u}^{(0)}) e_{xpq}(\mathbf{u}^{(0)})$, then the evolution law can be written in a compact form :

$$\dot{d} = \frac{2c_R}{\varepsilon} \left\langle 1 - \frac{\mathcal{G}_c^2}{\varepsilon^2 (Y - Y_f)^2} \right\rangle^{1/\alpha} \tag{38}$$

The microscopic length ε is present in the damage law and will be responsible for microstructural size effects.

We note that the expression (38) of the damage law is different from those obtained previously in dynamics for mode I microcrack propagation (Keita et al., 2014; Dascalu, 2018) or in quasi-statics for mode II microcracks (Wrzesniak et al., 2015). Its expression is closer to that obtained in mode III case (Atiezo and Dascalu, 2017) without considering contact and friction conditions. The damage evolution law (38) is the first approach of this type combining dynamics and friction effects on microcracks.

5. Local macroscopic behavior

The analysis of the local response predicted by the new damage model is performed in the present section. For the numerical implementation, the material parameters of the PMMA polymer are used : dynamic Young's modulus $E = 5.5\, GPa$, Poisson's ratio $\nu = 0.35$ and mass density $\rho = 1190\, kg/m^3$. Based on the estimation in Broberg (1987), where the mode II fracture toughness for PMMA was determined to be about 2.5 times the mode I toughness, we adopt for the critical fracture energy $\mathcal{G}_c = 2100 J/m^2$. Three values of the friction coefficient $\mu_f = 0$, $\mu_f = 0.25$ and $\mu_f = 0.5$ are considered in the

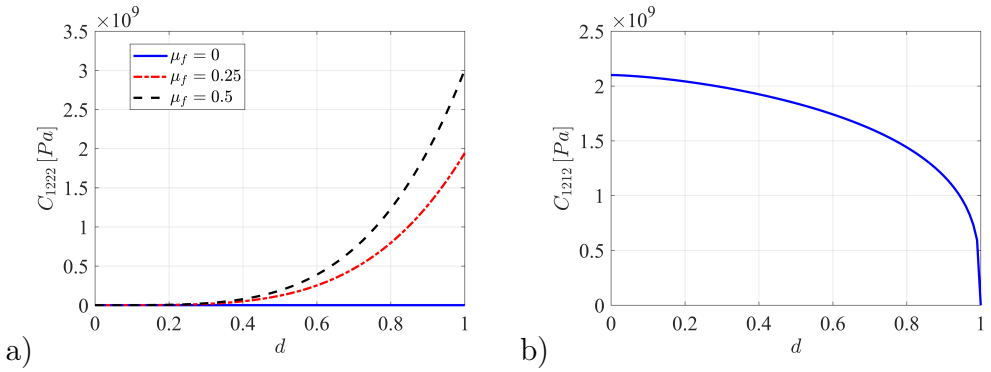

FIGURE 3: Effective moduli $C_{1222}(d)$ and $C_{1212}(d)$ for three values of the friction coefficient : $\mu_f = 0$, $\mu_f = 0.25$ and $\mu_f = 0.5$.

present analysis. The exponent for the approximation (35) of $g_2(v)$ is taken to be $\alpha = 1$.

5.1. Homogenized coefficients C_{mnpq} and I_{mnpq}

To calculate the homogenized coefficients C_{mnpq} and the integrals I_{mnpq} present in the damage law (37) the particular solutions of the unit cell problem (42-45) are needed. Finite Element computations with the commercial software Comsol Multiphysics (2015) are performed to obtain the corresponding numerical solutions. Some details on the unit cell problem formulation are given in the Appendix.

In order to obtain the dependence on the damage variable d, the cell problems were numerically solved for different crack lengths. With these solutions, the integral formulae (56-58) on the unit cell B and the two integrals in (61) on the edges of the crack CB were evaluated. The computations were performed for 20 values of the crack length d, ranging from 0 to 1. Then, the obtained numerical values of C_{mnpq} and I_{mnpq} were computed as functions

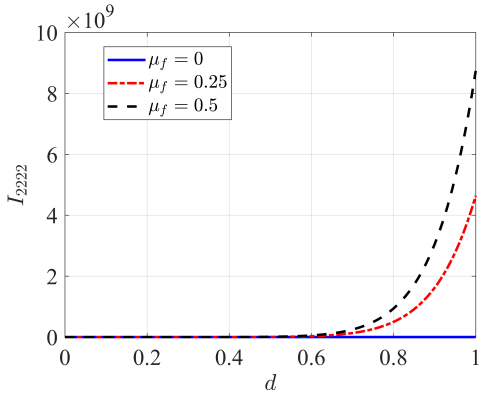

FIGURE 4: I_{2222} vs d for three values of the friction coefficient : $\mu_f = 0$, $\mu_f = 0.25$ and $\mu_f = 0.5$.

of d by polynomial interpolations. The first term in the expression (61) was obtained by derivation of the interpolated integral.

For $d = 0$, the effective coefficients are equal to the elastic coefficients of the undamaged material $C_{ijkl} = a_{ijkl}$, while for $d \neq 0$ the coefficients : $C_{1111} = a_{1111}$, $C_{1122} = C_{2211} = a_{1122}$, $C_{1112} = C_{1211} = 0$, $C_{2222} = a_{2222}$ are not affected by the variation of d. The computation of the integral terms in I_{ijkl} revealed that the only non-negligible coefficient is I_{2222}. In Figures 3 and 4 we represent, respectively, $C_{1222}(d)$, $C_{1212}(d)$ and $I_{2222}(d)$ corresponding to a crack orientation along the y_1-axis and for the three values of μ_f.

The effective coefficients C_{1222} and C_{1212} are shown in Figure 3. C_{1222} characterizes the influence of the compression deformation $e_{x22}(\mathbf{u}^{(0)})$ on the macroscopic shear stress $\Sigma_{12}^{(0)}$. In the absence of friction, there is no such influence on the shear stress response while, in the presence of friction, the compression influence the frictional resistance giving rise shear stresses. This effect is amplified by the value of the friction coefficient and also by the size

of the friction zone, controlled by the normalized microcrack length d. The two influences can be remarked in Figure 3a, the effective coefficient $C_{1222}(d)$ being an increasing function and having the highest values for $\mu_f = 0.5$.

As concerns the coefficient C_{1212}, the Figure 3b shows that it is a decreasing function of d and its behavior is not affected by the value of the friction coefficient. It represents the effect of the shear deformation of the unit cell on the macroscopic shear stress. The presence of microcracks makes easier the deformation of the cell and reduce the level of resulting shear stress. This explains the decrease of C_{1212} with respect to d. For a completely fractured cell, no shear stresses are generated since the two parts move freely.

The coefficient I_{2222} is represented in the Figure 4 as a function of damage d. Since these coefficients characterize the dissipation due to friction on the lips of microcracks, it is evident that they vanish for $\mu_f = 0$ and have higher values for large friction coeffcients. Moreover, $I_{2222}(d)$ is an increasing function since friction on larger microcracks involve more dissipation of energy. This dissipation mechanism will reduce the energy available for fracture and will delay the propagation of microcracks.

5.2. Local response analysis

Let us now study the local stress and damage response of the new model for a given strain history in a macroscopic point. The material parameters listed in the beginning of this section are used as an initial basis for the subsequent parametric studies. A shear strain history $e_{x12}(t)$ with constant strain rate $\dot{e}_{x12} = -8000/s$ and a fixed compression strain $e_{x22} = -5 \times 10^{-3}$ are given while the other strain components are vanishing.

In Figure 5 are represented the damage d and the stress $-\Sigma_{12}$ as functions

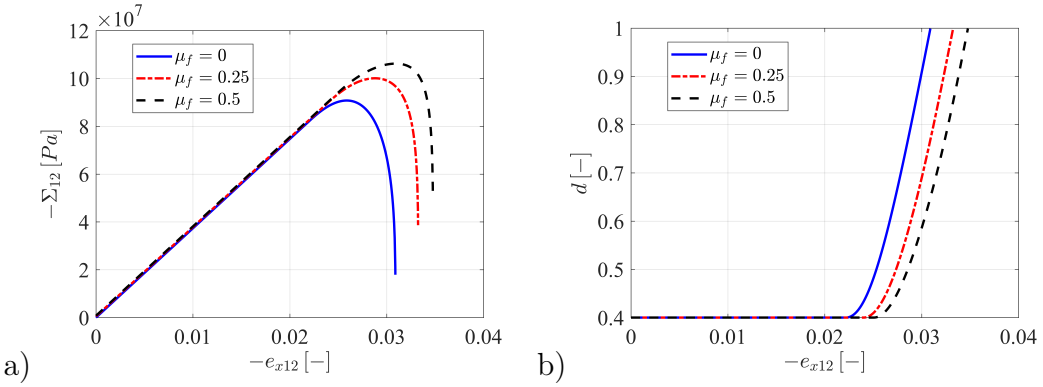

FIGURE 5: Stress $-\Sigma_{12}$ and damage d vs strain $-e_{x12}$ for three values of the friction coefficient : $\mu_f = 0$, $\mu_f = 0.25$ and $\mu_f = 0.5$.

of the applied strain $-e_{x12}$, for three values of the friction coefficient $\mu_f = 0$, $\mu_f = 0.25$, $\mu_f = 0.5$. The value of the initial damage is chosen $d_0 = 0.2$ and the microstructural length is $\varepsilon = 0.003\ m$. After the initial elastic regime, damage evolves and the stress-strain curve shows successive hardening and softening behavior up to complete failure. When the friction coefficient of microcracks increases, the necessary shear deformation to initiate the propagation is higher due to higher friction resistance. An important part of energy is dissipated by friction on the microcrack lips, reducing the amount of energy available for fracture. The initiation delay leads to the development of higher shear strength values.

Let us consider now the influence of the normal compression. Three different normal strain values : $e_{x22} = -10^{-3}$, $e_{x22} = -8 \times 10^{-3}$ and $e_{x22} = -1.5 \times 10^{-2}$ are considered and the corresponding responses are represented for the friction coefficient $\mu_f = 0.5$, the applied strain rate $\dot{e}_{x12} = -8000/s$, $\varepsilon = 5 \times 10^{-3}\, m$ and the initial damage $d_0 = 0.2$.

The Figure 6 shows the stress $-\Sigma_{12}$ and the damage d as a function of

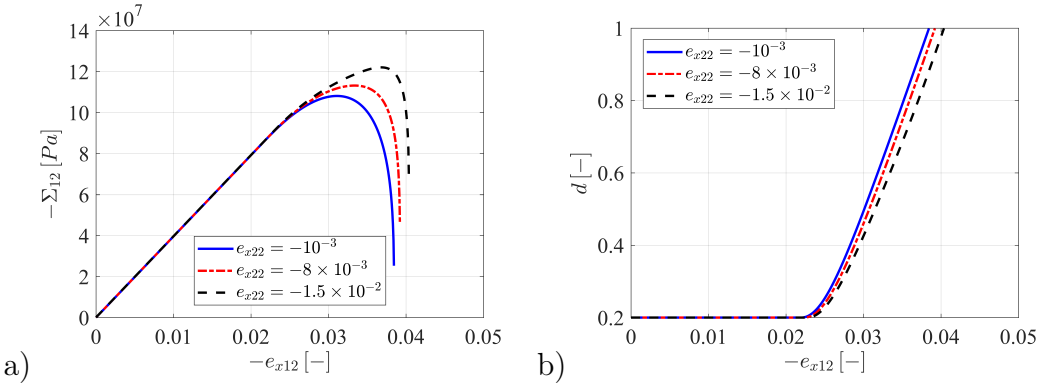

FIGURE 6: Stress $-\Sigma_{12}$ and damage d responses for three values of the compressive strain.

the strain $-e_{x12}$ for different values of e_{x22}. We observe that the increase of the compression strain produces a delay in the evolution of damage. In this case, the friction resistance is higher making the propagation of microcracks more difficult and leading to the development of higher values of the shear stress. The shear strength essentially depends on the normal compression, as a consequence of frictional sliding on microcracks, and is increasing with the normal strain. This effect is important for the reliability of structures subjected to shear deformations since the application of normal compression loadings increases the shear strength and may avoid catastrophic failure.

We analyse now the local macroscopic response for different values of the strain rate : $\dot{e}_{x12} = -100\ /s$, $\dot{e}_{x12} = -1000\ /s$, $\dot{e}_{x12} = -10000\ /s$. The stress curves $-\Sigma_{12}$ vs. $-e_{x12}$ and damage d vs $-e_{x12}$ are given in Figure 7 for a coefficient of friction $\mu_f = 0.5$ and for $\varepsilon = 2 \times 10^{-3}\, m$.

While the response is brittle for the first two values, the loading with the highest strain rate induces some ductility in the softening regime associated with a slight increase in strength. This is a typical inertial strain-rate effect,

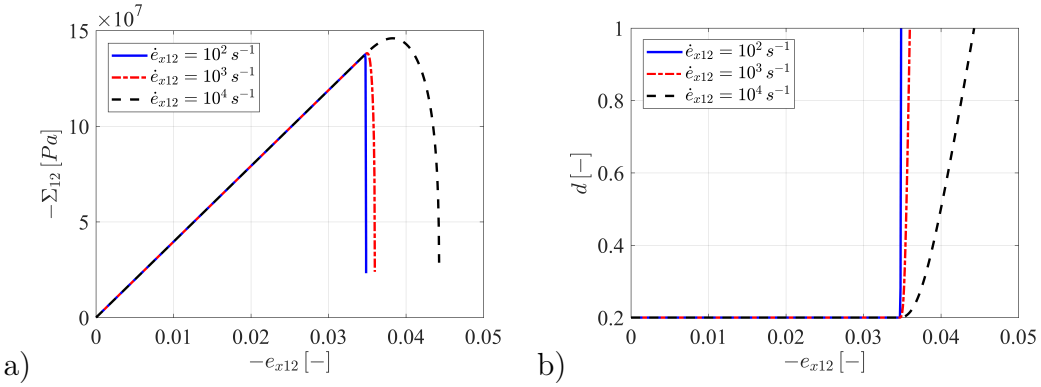

FIGURE 7: Stress $-\Sigma_{12}$ and damage d response for three values of the strain rate : $\dot{e}_{x12} = -100\ /s$, $\dot{e}_{x12} = -1000\ /s$, $\dot{e}_{x12} = -10000\ /s$.

also present in the absence of friction. It is essentially due to the formation of a non-negligible amount of kinetic energy near the crack lips which reduces the available energy for fracture. We note that this effect is less pronounced than in the case of opening of microcracks (Keita et al., 2014) where the amount of kinetic energy may be more important.

We also study the effect of the microstructural length on the local response. The tests were performed for the applied strain rate $\dot{e}_{x12} = -8000/s$ and $e_{x22} = -1 \times 10^{-3}$ and the coefficient of friction $\mu_f = 0.5$. Three sizes of microstructure were considered : $\varepsilon = 5 \times 10^{-3}\,m$, $\varepsilon = 5 \times 10^{-4}\,m$ and $\varepsilon = 5 \times 10^{-5}\,m$ and the results are presented in Figure 8. We observe that the shear strength increases and damage initiation is delayed as the size of the microstructure decreases. This is the typical Fracture Mechanics size effect transferred to the damage model at the macroscopic level : larger microcracks propagate much easier than smaller ones. The finer the microstructure, the stronger the material.

Finally, we consider the case of crack-velocity dependent fracture energy

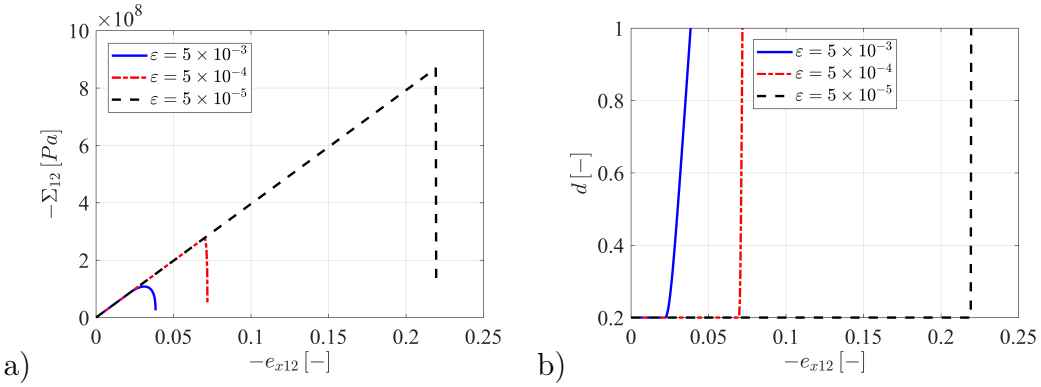

FIGURE 8: Stress $-\Sigma_{12}$ and damage d vs strain $-e_{x12}$ for micro-structural lengths : $\varepsilon = 5\times10^{-3}\,m$, $\varepsilon = 5\times10^{-4}\,m$ and $\varepsilon = 5\times10^{-5}\,m$.

$\mathcal{G}_c(v)$. As we will illustrate in the next section, this dependency is necessary to recover the experimental results. For mode I dynamic fracture, the dependency $\mathcal{G}_c(v)$ has been studied by different authors, e.g. Bjerke and Lambros (2003); Dalmas et al. (2013). To our knowledge, such results are not available for the mode II failure. Similarly to the opening mode case (Dascalu and Gbetchi, 2019), we consider the linear approximation $\mathcal{G}_c(v) = \mathcal{G}_{c0}(1 + a.v)$.

In Figure 9 the stress and damage curves are plotted for $\mathcal{G}_{c0} = 2100J/m^2$, for both $a = 0$ and $a = 0.01$. The other parameters are $\dot{e}_{x12} = -8000/s$, $e_{x22} = -1\times10^{-3}$, $\varepsilon = 1\times10^{-3}\,m$ and $\mu_f = 0.5$. As expected, the increase of the fracture energy with the velocity of the cracks leads to a damage delay and the corresponding peak stress increase. The influence of non-vanishing a will be important for the macroscopic simulations presented in the next section.

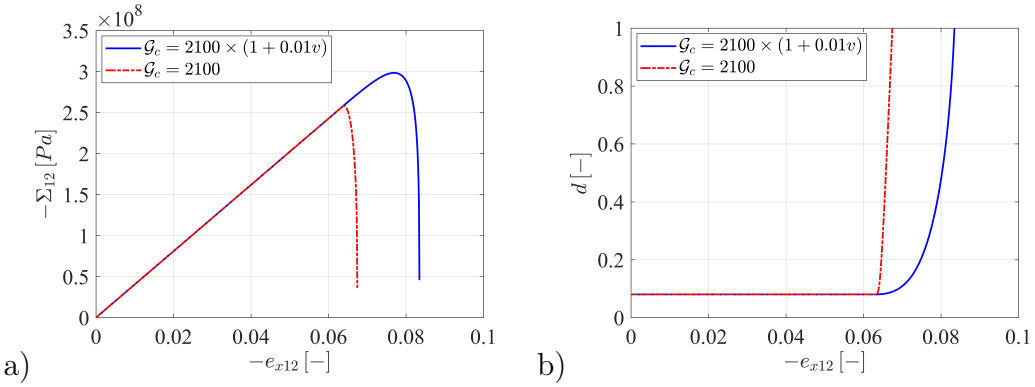

FIGURE 9: Stress $-\Sigma_{12}$ and damage d vs strain $-e_{x12}$, for constant and crack-velocity dependent fracture energy.

6. Numerical simulations of mode II failure of PMMA samples under impact

We investigate here the capacity of the damage model to reproduce quantitatively the experimental results in Ravi-Chandar et al. (2000) concerning the rapid shear failure of PMMA samples under impact loading. The authors showed that, by increasing the impact speed, the failure dominated by normal stress changes to a shear stress dominated failure oriented in the loading direction. Since the fracture toughness in mode II is much larger than in mode I (Broberg, 1987; Ravi-Chandar et al., 2000), side-grooved specimens are used in order to promote the shear failure mode.

The geometry of the specimen is given in Figure 10a. The dimensions are defined as $W = 100\,mm$, $2H = 400\,mm$ and $T = 6.35\,mm$. The grooves at both sides of the sample have the depth $D_g = 1.5\,mm$ and the height $H_g = 3.2\,mm$. The length of the initial notch is $l = 19\,mm$ and its thickness is $0.3\,mm$. As shown Figure 10a, asymmetric impact loading with the velocity

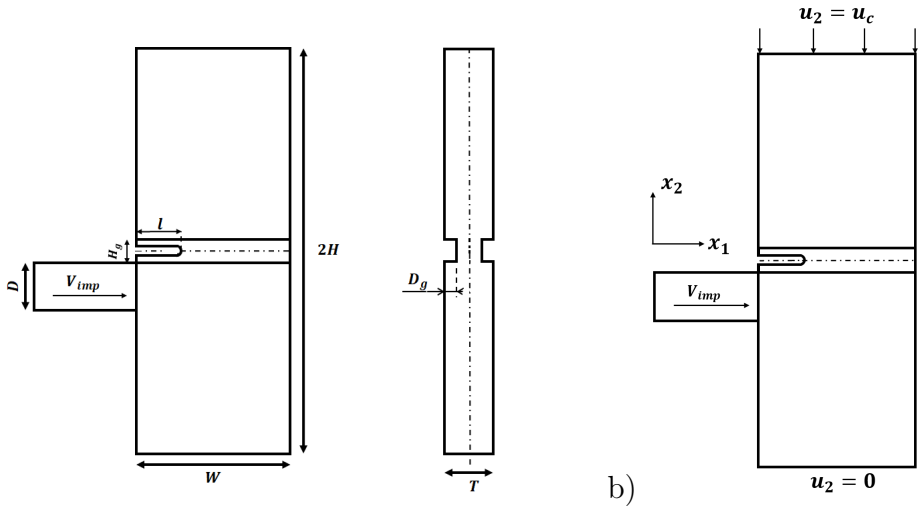

FIGURE 10: Geometry of the specimen and applied loadings : a) impact, b) impact and normal compression.

$V_{imp} = 60\,m/s$ is applied over a zone of $D = 50\,mm$, corresponding to the diameter of the projectile used for the experiments.

The applied loading generates a dominant shear stress state at the tip of the initial notch and initiate the shear failure along the groove. The dimensions of the specimen are such that, during the first $100\,\mu s$, there is not effect of the reflected waves from the far boundaries, the only loading being that of the projectile. The observations in Ravi-Chandar et al. (2000) show the formation of a shear crack along the groove and a kinked mode I crack inclined at some angle with respect to the loading direction. This latter opening crack was missing in some experiments, only the shear crack being present. Since the model developed in the present contribution is based on mode II microcracks, our aim is to reproduce the formation of the macroscopic shear fracture.

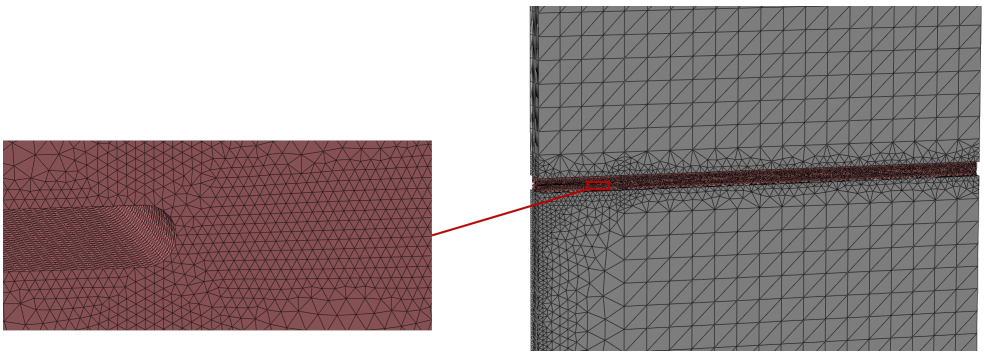

FIGURE 11: Details of the mesh used in the FE simulations.

The numerical values of the dynamic Young's modulus E, the Poisson's ratio ν and the mass density ρ for the PMMA material are given in the Table 1. Also given are the friction coefficient μ_f, the microstructural length ε, the initial damage d_0 and the exponent α in the approximation (35) of $g_2(v)$. The critical fracture energy is assumed to be velocity dependent $\mathcal{G}_c = \mathcal{G}_{c0} \times (1 + a.v)$. The choice of the parameters is discussed below.

The damage model has been implemented in the commercial Finite Element software Abaqus (2013), as a VUMAT user material subroutine. Dynamic elasticity computations can be performed in Abaqus Explicit with the resolution of the damage equation in the user subroutine. On a time step and for given strain increments in an integration point of the FE mesh, the damage law (38) is numerically integrated using a Euler forward scheme. Only

TABLE 1: Parameters used in the computations

$E\,(GPa)$	$\nu\,(-)$	$\rho\,(kg/m^3)$	$\mu_f\,(-)$	$\varepsilon\,(m)$	$d_0\,(-)$	$\alpha\,(-)$	$\mathcal{G}_{c0}\,(J/m^2)$	$a\,(s/m)$
5.5	0.35	1190	0.5	8×10^{-5}	0.08	1	2100	0.0075

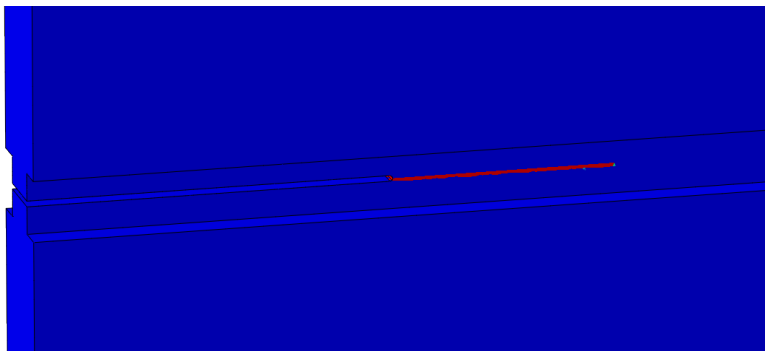

FIGURE 12: Damage band propagation inside the groove.

the in-plane strain components are considered in the expression of the energy terms Y and Y_f in the damage law (38).

In order to account for the effect of the grooves on the initiation of the shear failure, a 3D FE discretization is adopted. A FE mesh is constructed using four nodes tetrahedral linear elements C3D4. The details of the mesh are given in Figure 11. A refinement is considered in the groove, along the expected path of the damage band, with the element size of $5 \times 10^{-2}\, mm$.

Under the impact loading, damage localization occurs starting from the tip of the notch and the damage band propagates in the groove. The complete failure corresponds to a critical value of the damage parameter $d = 0.99$ at the integration point. When this state is reached, the respective element is deleted and unilateral contact with friction conditions are introduced between the new formed boundaries of the macroscopic crack. In this evolution, the damage localization is a consequence of the softening response of the model (Dascalu, 2017) and transition to discontinuous crack is performed numerically at complete failure. Other approaches, like the one in Zhao et al. (2018) where the localization process is described with a traction-based

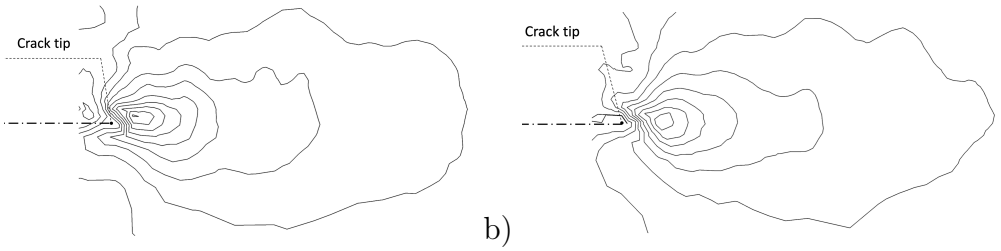

FIGURE 13: Lines of constant shear stress Σ_{12} at : a) $40\,\mu s$ and b) $60\,\mu s$. The absolute values of Σ_{12} are increasing when approaching the tip of the damage band.

friction-damage law on the newly formed macrocrack, may be adapted in future studies to the dynamic damage model proposed in the present contribution.

A typical evolution of the damage band initiated at the notch tip and evolving in the groove is represented in Figure 12. The trajectory is relatively straight, in the loading direction. This corresponds to the experimental observations of the shear crack by Ravi-Chandar et al. (2000). The authors also give the tip positions at different instants of time ; they are represented in Figures 14-17 with red square symbols.

In Figure 13 the lines of constant shear stress Σ_{12} are represented near the tip of the damage band at $40\,\mu s$ and $60\,\mu s$, respectively. When approaching the tip, the absolute values of Σ_{12} are increasing, with a maximum in the immediate vicinity of the damage front. With respect to the angle at the tip, they are maximal approximately on the (horizontal) damage line, ahead of the tip. This distribution is characteristic to dominant mode II crack propagation (e.g. Ravi-Chandar, 2004).

To explore the possibility of reproducing the experimental data for the

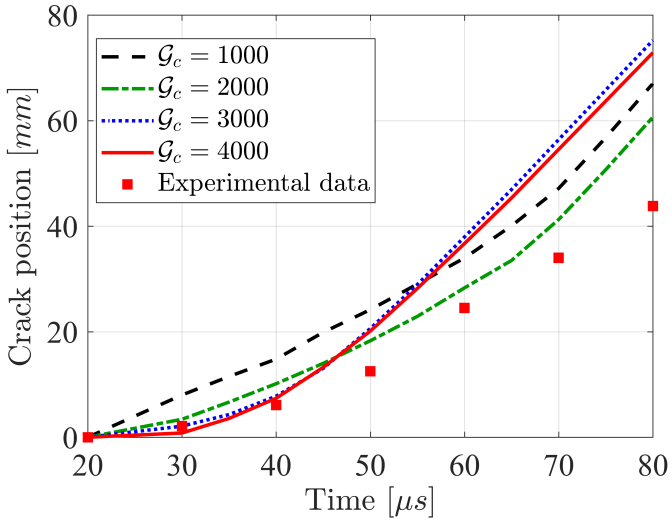

FIGURE 14: Variation of the crack-tip position with time for constant values of $\mathcal{G}_c$.

crack-tip evolution, we first considered the case of constant fracture energy $\mathcal{G}_c = \mathcal{G}_{c0}$. In Figure 14 the variation of the crack tip position with time is represented for four constant values of $\mathcal{G}_c$. A tendency of approaching the experimental points is observed when one increases the fracture energy but this is effective only on the interval up to $40\,\mu s$. For large values of $\mathcal{G}_c$, the propagation is more rapid. Since the increase of the critical energy first delayed the propagation, much more energy is stored in the sample leading to more rapid propagation in a second stage.

In these simulations the value of the microstructural length is $\varepsilon = 8 \times 10^{-5}\,m$. Note that this value is close to the one considered for the mode I failure $\varepsilon = 6 \times 10^{-5}\,m$ in the compact compression specimen impact test Dascalu and Gbetchi (2019). The particular influence of $\mathcal{G}_c$ in Figure 14 is also obtained when the critical energy is kept constant but the length ε

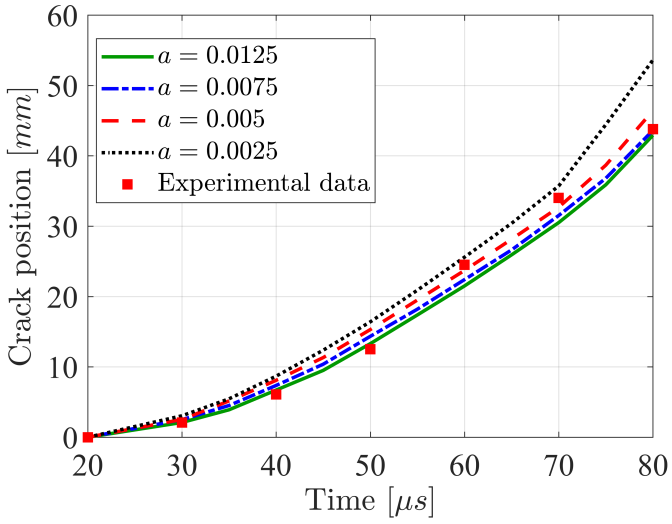

FIGURE 15: Crack-tip position vs time for different values of a and variable fracture energy $\mathcal{G}_c = 2100 \times (1 + a.v)$.

is decreased. For smaller microstructures, the propagation is also delayed initially and the same acceleration effect in the later stage is retrieved.

The next step of our investigation is to consider velocity-dependent fracture energy $\mathcal{G}_c = \mathcal{G}_{c0} \times (1 + a.v)$. For the initial value $\mathcal{G}_{c0} = 2100\, J/m^2$ was found to be a good choice. Relatively good approximations of the experimental data are obtained for a in the range $0.0075 - 0.0125\, s/m$. We note that the value $\mathcal{G}_{c0} = 2100\, J/m^2$ is consistent with the estimation of Broberg (1987) who determined that the ratio between mode II and mode I fracture toughness is about 2.5. This would correspond to a mode I fracture energy of $336\, J/m^2$ which is in the range of acceptable values for the PMMA material.

The predicted crack tip position at different instants of time and for $a = 0.0075\, s/m$ is represented in Figure 17. This rapid evolution is typical for a shear crack. The crack velocity is increased in $80\, \mu s$ up to a value close

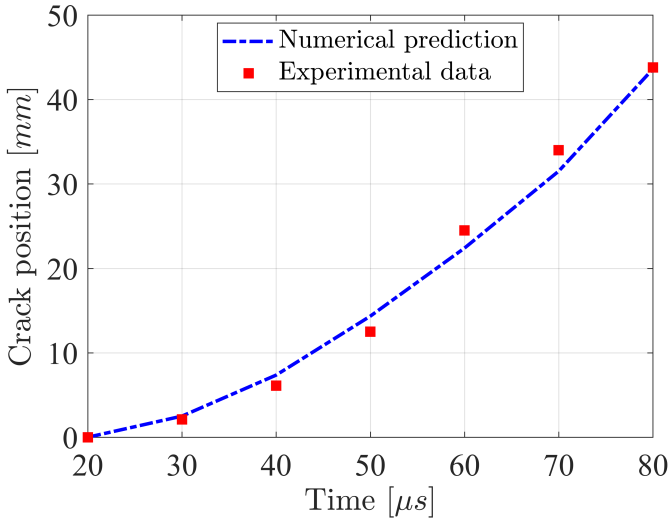

FIGURE 16: Crack-tip position vs time for $\mathcal{G}_c = 2100 \times (1 + 0.0075.v)$.

to the Rayleigh wave speed, which is $1222.1\, m/s$ for the considered material parameters. This corresponds to the mesures reported in Ravi-Chandar et al. (2000). It is known that mode I cracks usually do not evolve up to the theoretical limit which is the Rayleigh wave velocity, but have a lower limit speed due to the development of micro-branching instabilities (Ravi-Chandar, 2004).

In order to evaluate the influence of the friction on fracture evolution, we also simulated the impact test in the case of frictionless contact $\mu_f = 0$ on microcracks. For the sake of comparison, we plotted in Figure 17 the crack-tip positions vs time for $\mu_f = 0$ and $\mu_f = 0.5$, respectively. It can be remarked that the presence of friction slows down the fracture evolution. This influence at the structural level is related to that revealed by the local analysis and shows the necessity of including frictional effects on microcracks

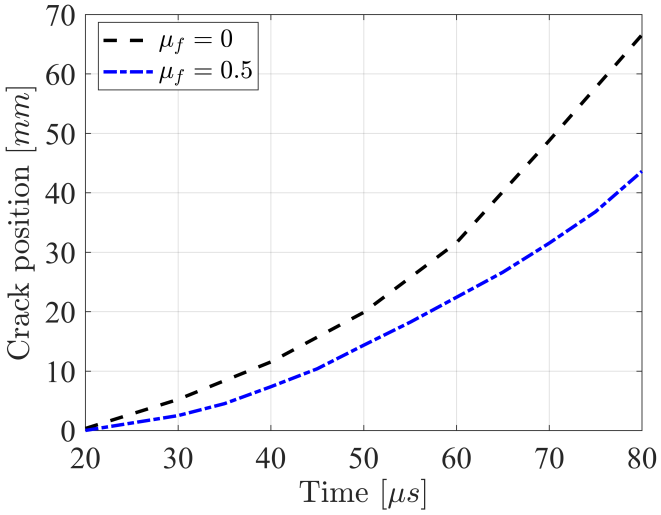

FIGURE 17: Crack-tip position vs time for $\mu_f = 0$ and $\mu_f = 0.5$.

in the modeling of failure of quasi-brittle materials.

We finally study the influence of the normal compression on the macroscopic crack growth. For this, in addition to the impact loading, a normal displacement is applied on the top boundary of the specimen while the bottom is blocked in the vertical direction x_2. No constraints are imposed in the impact direction x_1 on these two boundaries. The new loading is illustrated in Figure 10b. In order to have an effective compression in the groove before impact, the applied displacement is chosen in the form :

$$u_2(t) = \frac{u_c}{t_0} t \quad \text{for } t \leq t_0 \quad ; \quad u_2(t) = u_c \quad \text{for } t \geq t_0 \tag{39}$$

with $t_0 = 100\,\mu s$ and the impact velocity $V_{imp} = 60\,m/s$ is applied starting from $t_1 = 200\,\mu s$.

In Figure 18, the crack tip advancement has been represented for different values of the applied normal displacement $u_c = 0\,m$, $u_c = -0.0025\,m$,

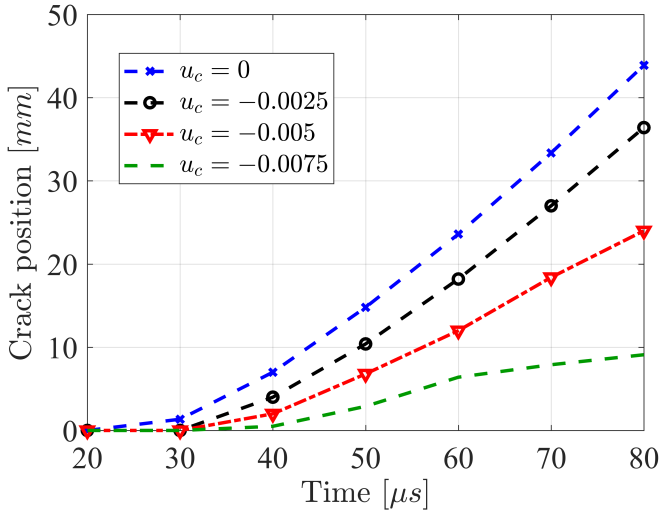

FIGURE 18: Crack-tip position vs time for different values of the applied normal displacement u_c at the top of the specimen.

$u_c = -0.005\,m$ and $u_c = -0.0075\,m$, respectively. As expected, when u_c is increased the fracture propagation is delayed as a consequence of the increased frictional resistance. We retrieve at the level of the macrostructure the influence of the normal compression discussed in the local analysis. This influence cannot be captured using a damage model not accounting for frictional effects.

Conclusions

A new dynamic damage model taking into account the dissipation due to friction on the lips of microcracks has been proposed. The damage evolution law is obtained by asymptotic homogenization from a microscopic Griffith-type propagation criterion in mode II.

Unilateral contact with friction conditions have been assumed on the lips

of microcracks. The macroscopic damage law contains a length parameter characterizing the mutual distance between neighbor microcracks. Microstructural size effects, strain-rate sensitivity and friction influence are analyzed at the local and structural levels.

Numerical simulations of the impact test on PMMA samples are presented. For high impact velocities, the shear failure mode is activated in grooved specimens. It was found that the model predictions are in good agreement with the experimental data.

Further developments of the present model may explore the possibility to reproduce simultaneous mode I and mode II propagation by combination with the damage model in Keita et al. (2014); Dascalu (2018), the prediction of the intersonic shear failure by replication of the experiments in Rosakis et al. (2000) or the inclusion of frictional heating effects using an approach similar to that developed in Dascalu and Gbetchi (2019) for mode I failure.

Acknowledgements

The research leading to these results has received funding from the European Union's Horizon 2020 Programme (Excellent Science, Marie-Sklodowska-Curie Actions) under REA grant agreement 675602 (Project OUTCOME).

Appendix : Computation of the effective coefficients C_{ijkl} and I_{mnpq}

We provide here the details concerning the computation of the homogenized coefficients C_{ijkl} and I_{mnpq} appearing in the formulation of the macroscopic elasto-damage problem. As explained in Wrzesniak et al. (2015), a particular system of generators for the cell problem is necessary to respect

the frictional contact conditions on the crack lips. The construction is specific to the present orientation of microcracks.

Following the method in Wrzesniak et al. (2015), we choose a system of generators $\mathbf{E}^{pq}$ in the form :

$$\mathbf{E}^{11} = \begin{pmatrix} -1/\beta & 0 \\ 0 & 0 \end{pmatrix};\ \mathbf{E}^{12} = \begin{pmatrix} 0 & -1/\beta \\ -1/\beta & -1/2\beta \end{pmatrix};\ \mathbf{E}^{22} = \begin{pmatrix} 0 & -1/\beta \\ -1/\beta & -1/\beta \end{pmatrix} \tag{40}$$

such that the macroscopic strains can be written as a linear combination of these elements :

$$e_{xij}(\mathbf{u}^{(0)}) = \alpha_{pq}(\mathbf{u}^{(0)})E_{ij}^{pq} \tag{41}$$

where $\alpha_{pq}(\mathbf{u}^{(0)})$ are linear combinations of the macroscopic strain components : $\alpha_{11}(\mathbf{u}^{(0)}) = -\beta e_{x11}(\mathbf{u}^{(0)})$, $\alpha_{12}(\mathbf{u}^{(0)}) = \alpha_{21}(\mathbf{u}^{(0)}) = \beta(e_{x22}(\mathbf{u}^{(0)}) - e_{x12}(\mathbf{u}^{(0)}))$ and $\alpha_{22}(\mathbf{u}^{(0)}) = \beta(e_{x12}(\mathbf{u}^{(0)}) - 2e_{x22}(\mathbf{u}^{(0)}))$. In the sommation terms of the relation (41) we take $\mathbf{E}^{21} = \mathbf{E}^{12}$. The applied macroscopic strains in the computations of the cell-problem solutions are adjusted with the constant $\beta = 800$ in order to maintain the numerical contact conditions, imposed through a penalty method, and avoid penetrations of the crack lips due to high compressive loadings.

If the vectors $\boldsymbol{\eta}^{pq}(\mathbf{y}, d)$ are particular solutions, corresponding to $e_{xij}(\mathbf{u}^{(0)}) = E_{ij}^{pq}$, of the cell problem :

$$\frac{\partial}{\partial y_i}(a_{ijkl}e_{ykl}(\boldsymbol{\eta}^{pq})) = 0 \quad \text{in} \quad B \tag{42}$$

$$[a_{ijkl}e_{ykl}(\boldsymbol{\eta}^{pq})N_j] = -\left[(a_{ijkl}E_{kl}^{pq})N_j\right] \ \text{ on } \ CB \tag{43}$$

$$N_i a_{ijkl}(e_{ykl}(\boldsymbol{\eta}^{pq}) + E_{kl}^{pq})N_j < 0 \ \text{ on } \ CB \tag{44}$$

$$|T_i a_{ijkl}(e_{ykl}(\boldsymbol{\eta}^{pq}) + E_{kl}^{pq})N_j| = -\mu_f N_i a_{ijkl}(e_{ykl}(\boldsymbol{\eta}^{pq}) + E_{kl}^{pq})N_j \ \text{ on } \ CB \tag{45}$$

then the general solution $\mathbf{u}^{(1)}$ can be written as the linear combination :

$$\mathbf{u}^{(1)}(\mathbf{x},\mathbf{y},t) = \boldsymbol{\eta}^{pq}(\mathbf{y},d(t))\alpha_{pq}(\mathbf{x},t) \tag{46}$$

For the numerical solution, it is preferable to use the change of function from η_i^{pq} to v_i, with $\eta_i^{pq} = v_i^{pq} - E_{ij}^{pq}y_j$. With this change of variable, the periodicity conditions on the outer edges of the cell become :

$$(\mathbf{v}^{pq} - \mathbf{E}^{pq}\mathbf{y})^+ = (\mathbf{v}^{pq} - \mathbf{E}^{pq}\mathbf{y})^- \tag{47}$$

where $\mathbf{y}$ is the position vector and $\pm$ defines the opposite edges of the unit cell. With this change, the problem (42-45) becomes :

$$\frac{\partial}{\partial y_i}(a_{ijkl}e_{ykl}(\mathbf{v}^{pq})) = 0 \quad \text{in} \quad B \tag{48}$$

$$[a_{ijkl}e_{ykl}(\mathbf{v}^{pq})N_j] = 0 \ \text{ on } \ CB \tag{49}$$

$$N_i a_{ijkl}e_{ykl}(\mathbf{v}^{pq})N_j < 0 \ \text{ on } \ CB \tag{50}$$

$$|T_i a_{ijkl}e_{ykl}(\mathbf{v}^{pq})N_j| = -\mu_f N_i a_{ijkl}e_{ykl}(\mathbf{v}^{pq})N_j \ \text{ on } \ CB \tag{51}$$

The condition of continuity of the normal displacements on the crack lips becomes :

$$[\mathbf{v}^{pq}.\mathbf{N}] = 0 \ \text{ on } \ CB \tag{52}$$

The particular solutions $\mathbf{v}$ of this problem are determined for given values of the variable d.

Let us provide now details for the computation of the effective coefficients C_{ijmn} in (28). Replacing the relations (41) and (46) in (26), we get :

$$\Sigma_{ij}^{(0)} = \frac{1}{|B|}\int_B a_{ijkl}(E_{kl}^{mn} + e_{ykl}(\boldsymbol{\eta}^{mn})dy\, \alpha_{mn}(\mathbf{u}^{(0)}) \tag{53}$$

which can be rewritten :

$$\Sigma_{ij}^{(0)} = C_{ijmn}^{\alpha} \alpha_{xmn}(\mathbf{u}^{(0)}) \tag{54}$$

with the coefficients

$$C_{ijmn}^{\alpha} = \frac{1}{|B|} \int_B a_{ijkl}(E_{kl}^{mn} + e_{ykl}(\boldsymbol{\eta}^{mn}))dy \tag{55}$$

Since $|B| = 1$, it will be omitted in what follows. Using the link between e_{xij} and α_{pq} in (54) allows to rewrite the macroscopic stress in order to obtain the homogenized constitutive relation (28) with the effective coefficients

$$C_{ij11} = -\int_B \beta a_{ijkl}(E_{kl}^{11} + e_{ykl}(\boldsymbol{\eta}^{11}))dy \tag{56}$$

$$C_{ij12} = \int_B \frac{\beta}{2} a_{ijkl}((E_{kl}^{22} + e_{ykl}(\boldsymbol{\eta}^{22})) - 2(E_{kl}^{12} + e_{ykl}(\boldsymbol{\eta}^{12})))dy \tag{57}$$

$$C_{ij22} = \int_B 2\beta a_{ijkl}((E_{kl}^{12} + e_{ykl}(\boldsymbol{\eta}^{12})) - (E_{kl}^{22} + e_{ykl}(\boldsymbol{\eta}^{22})))dy \tag{58}$$

As concerns the energy relation (36), following the analysis in Wrzesniak et al. (2015) one ontains it in terms of $\alpha_{pq}(\mathbf{u}^{(0)})$:

$$\left(\frac{\mathcal{G}^{\varepsilon}}{\varepsilon} + (\frac{1}{2} \frac{\partial C_{mnpq}^{\alpha}}{\partial d} + I_{mnpq}^{\alpha}) \alpha_{mn}(\mathbf{u}^{(0)}) \alpha_{pq}(\mathbf{u}^{(0)}) \right) \dot{d} = 0 \tag{59}$$

where

$$\begin{aligned} I_{mnpq}^{\alpha} = & \frac{1}{2} \frac{d}{dd} \int_{CB} a_{ijkl}(E_{kl}^{mn} + e_{ykl}(\boldsymbol{\eta}^{mn})) N_j[\eta_i^{pq}] ds_y \\ & - \int_{CB} a_{ijkl}(E_{kl}^{mn} + e_{ykl}(\boldsymbol{\eta}^{mn})) N_j[\frac{d\eta_i^{pq}}{dd}] ds_y \end{aligned} \tag{60}$$

And adopting the previous change of variables, we can rewrite the expression (60) as a function of v_i^{pq} :

$$I_{mnpq}^{\alpha} = \frac{1}{2} \frac{d}{dd} \int_{CB} a_{ijkl} e_{ykl}(\mathbf{v}^{mn}) N_j[\mathrm{v}_i^{pq}] ds_y - \int_{CB} a_{ijkl} e_{ykl}(\mathbf{v}^{mn}) N_j[\frac{d\mathrm{v}_i^{pq}}{dd}] ds_y \tag{61}$$

To express the coefficients I_{mnpq} as a function of I^{α}_{mnpq}, we calculate the expression of $I^{\alpha}_{mnpq}\alpha_{mn}(\mathbf{u}^{(0)})\alpha_{pq}(\mathbf{u}^{(0)})$ in the law (59), depending on the strains $e_{xmn}(\mathbf{u}^{(0)})$, to obtain the equivalent form (36).

The numerical evaluation of the integrals shows that the following terms can be neglected : I^{α}_{1111}, I^{α}_{1112}, I^{α}_{1122}, I^{α}_{2211}, I^{α}_{1211}. Using the expressions of the strains $\alpha_{11} = -\beta e_{x11}$, $\alpha_{12} = \beta(e_{x22} - e_{x12})$, $\alpha_{22} = \beta(e_{x12} - 2e_{x22})$ one obtains :

$$I^{\alpha}_{mnpq}\alpha_{mn}(\mathbf{u}^{(0)})\alpha_{pq}(\mathbf{u}^{(0)}) = \beta^2(-2I^{\alpha}_{2222} + 6I^{\alpha}_{1222} + 6I^{\alpha}_{2212} - 8I^{\alpha}_{1212})e_{x12}(\mathbf{u}^{(0)})e_{x22}(\mathbf{u}^{(0)}) + 4\beta^2(I^{\alpha}_{2222} - I^{\alpha}_{1222} - I^{\alpha}_{2212} + I^{\alpha}_{1212})(e_{x22}(\mathbf{u}^{(0)}))^2 + \beta^2(I^{\alpha}_{2222} - 2I^{\alpha}_{1222} - 2I^{\alpha}_{2212} + 4I^{\alpha}_{1212})(e_{x12}(\mathbf{u}^{(0)}))^2 \quad (62)$$

From this last equation (62), we deduce the necessary coefficients for evaluating the term $Y_f = I_{mnpq}e_{xmn}(\mathbf{u}^{(0)})e_{xpq}(\mathbf{u}^{(0)}))$ in the damage law as :

$$\begin{aligned} I_{1222} + I_{2212} &= \frac{\beta^2}{2}(-2I^{\alpha}_{2222} + 6I^{\alpha}_{1222} + 6I^{\alpha}_{2212} - 8I^{\alpha}_{1212}) \\ I_{2222} &= 4\beta^2(I^{\alpha}_{2222} - I^{\alpha}_{1222} - I^{\alpha}_{2212} + I^{\alpha}_{1212}) \\ I_{1212} &= \frac{\beta^2}{4}(I^{\alpha}_{2222} - 2I^{\alpha}_{1222} - 2I^{\alpha}_{2212} + 4I^{\alpha}_{1212}) \end{aligned} \quad (63)$$

References

ABAQUS 6.13, 2013. Analysis User's Manual. Dassault Systems Simulia Corporation, RI, USA.

Andrieux S., Bamberger Y., Marigo J-J., 1986. Un modele de materiau microfissure pour les betons et les roches. J. Méc. Theor. Appl., vol. 5, p.471-513.

Archer, J.S., Lesser, A.J., 2010. Shear band formation and mode II fracture of polymeric glasses. J. Polym. Sci. B : Polymer Physics 49, 103-114.

Ashby, M.F., Hallam, S.D., 1986. The failure of brittle solids containing small cracks under compressive stress states. Acta Metall. 34, 497-510.

Atiezo M.K., Dascalu C., 2017. Antiplane two-scale model for dynamic failure. Int J. Fracture, vol. 206, 195-214.

Bakhvalov, N., Panasenko, G., 1989. Homogenization : Averaging Processes in Periodic Media, Kluwer Academic Publishers Group, Dordrecht.

Bazant, Z.P., Caner, F.C. 2014. Impact comminution of solids due to local kinetic energy of high shear strain rate : I. Continuum theory and turbulence analogy, II. Microplane model and verification, J. Mech. Phys. Solids, 64, 223-248.

Benssousan, A., Lions, J., Papanicolaou, G., 1978. Asymptotic Analysis for Periodic Structures, Kluwer Academic Publisher, Amsterdam.

Bhatt, H., Rosakis, A., Sammis, G., 2011. A micro-mechanics based constitutive model for brittle failure at high strain rates. J. Appl.Mech. 79(3), 1016-28.

Bjerke, T. W., 2002. Thermomechanical Behavior of Amorphous Polymers During High-Speed Crack Propagation, Ph. D. Dissertation, University of Delaware, Newark, DE.

Bjerke, T. W., Lambros, J., 2003. Heating During Shearing and Opening Dominated Dynamic Fracture of Polymers, Exp. Mech. 42, 107-114.

Broberg, KB, 1987, On crack paths. Engineering Fracture Mechanics, vol. 28, 5-6, 663 - 679

Broberg, K.B.,1989. The near-tip field at high crack velocities. Int. J. Fract. 39,1-13.

Broberg, K.B.,1995. Intersonic mode II crack expansion. Arch. Mech. 47(5), 859-871.

Broberg K. B., 1999. Cracks and fracture, Academic Press, San Diego.

Burridge, R., Conn, G., Freund, L.B., 1979. The stability of a rapid mode II shear crack with finite cohesive traction. J. Geophys. Res. 85(B5), 2210-2222.

Comsol Multiphysics, User's Guide, Version 5.2 (2015).

Dalmas, D., Guerra, C., Scheibert, J., Bonamy, D., 2013. Damage mechanisms in dynamic fracture of nominally brittle polymers, Int. J. Fract. 184, 93-111.

Dascalu, C., Bilbie, G., Agiasofitou E., 2008. Damage and size effect in elastic solids : A homogenization approach. Int. J. Solids Struct. 45, 409-430.

Dascalu, C., François, B., Keita, O., 2010. A two-scale model for subcritical damage propagation. Int. J. Solids Struct. 47, 493-502.

Dascalu, C., Dobrovat A., Tricarico M., 2010. On a 3D micromechanical damage model, International Journal of Fracture vol. 166, 153-162.

Dascalu, C., 2017. Dynamic localization of damage and microstructural length influence. Int. J. Damage Mech. 28, 1190-1218.

Dascalu, C., 2018. Multiscale modeling of rapid failure in brittle solids : branching instabilities. Mech. Mater., 116, 77-89.

Dascalu, C., Gbetchi K., 2019. Dynamic evolution of damage by microcracking with heat dissipation. Int. J. Solids Struct. vol. 174-175, 128-144.

Denoual, C., Hild, F., 2000. A damage model for the dynamic fragmentation of brittle solids. Comput. Methods Appl. Mech. Eng. 183, 247-258.

Dobrovat A., Dascalu, C., Hall S., 2015. Computational modeling of damage based on micro-crack kinking. Int. J. Multiscale Comput. Engng., vol. 13, 201-217.

Forquin, P., Hild, F., 2010. A probabilistic damage model of the dynamic fragmentation process in brittle materials. Adv. Appl. Mech. 44, 1-72.

François, B., Dascalu, C., 2010. A two-scale time-dependent damage model based on non-planar growth of micro-cracks, J. Mech. Phys. Solids 58, 1928-1946.

Freund, L.B., 1979. The mechanics of dynamic shear crack propagation. J. Geophys. Res. 84, 2199-2209.

Freund L.B., 1998. Dynamic fracture mechanics, Cambridge University Press.

Gambarotta, L., Lagomarsino S., 1993. A microcrack damage model for brittle materials. Int. J. Solids Struct, 30(2), 177-198.

Halm D., Dragon A., 1998. An anisotropic model of damage and frictional sliding for brittle materials, European Journal of Mechanics A Solids, Volume : 17, 439-460.

Horii, H., Nemat-Nasser, S., 1986. Brittle failure in compression : splitting, faulting and brittle-ductile transition. Philos. Trans. Roy. Soc. London 319, 337-374.

Huang, C., Subhash, G., Vitton, S.J., 2002. A dynamic damage growth model for uniaxial compressive response of rock aggregates. Mech. Mater. 34, 267-277.

Kachanov, L.M., 1982. A microcrack model of rock inelasticity - Part I : frictional sliding on microcracks ; Part II : propagation of microcracks. Mech. Mater. 1, 19-41.

Keita, O., Dascalu, C., François B., 2014. A two-scale model for dynamic damage evolution. J. Mech. Phys. Solids. 64, 170-183.

Lawn, B.R., Marshall D.B., 1998. Nonlinear stress-strain curves for solids containing closed cracks with friction. J. Mech. Phys. Vol.46, No. 1, 85-113.

Lee, X., Ju, J.W., 1991. Micromechanical Damage Model for Brittle solids - II : Compressive Loadings, J. Engrg. Mech., ASCE, 117, 1515-1536.

Li, T., Marigo, J.J., Guilbaud, D., Potapov, S., 2016. Numerical investigation of dynamic brittle fracture via gradient damage models, Adv. Model. Simul. Eng., 3 :26, 1-26.

Leguillon D., Sanchez-Palencia E.,1982. On the behaviour of a cracked elastic body with (or without) friction. J. Mech. Theor. Appl. 1, 195-209.

Markenscoff, X., Dascalu, C., 2012. Asymptotic homogenization analysis for damage amplification due to singular interaction of microcracks. J. Mech. Phys. Solids 60, 1478-1485.

Nemat-Nasser, S., and Obata M., 1988. A microcrack model of dilatancy in brittle material. J. of Applied Mechanics, 55, 24-35.

Nemat-Nasser, S., Deng, H., 1994. Strain-rate effect on brittle failure in compression. Acta Metall. Mater. 42, 1013-1024.

Paliwal, B., Ramesh, K. T., 2008, An Interacting Micro-Crack Damage Model for Failure of Brittle Materials Under Compression, J. Mech. Phys. Solids, 56(3), 896-923.

Ravi-Chandar, K., Lu J., Yang B., Zhu Z., 2000. Failure mode transitions in polymers under high strain rate loading. Int. J. Fracture, 101, 33-72.

Ravi-Chandar, K., 2004. Dynamic fracture. Boston. Elsevier.

Ravichandran, G., Subhash, G., 1995. A micromechanical model for high strain rate behavior of ceramics. Int. J. Solids Struct. 32, 2627-2646.

Rosakis, A. J., O. Samudrala, and D. Coker, 1999. Cracks Faster Than the Shear Wave Speed. Science, 284, pp. 1337-1340.

Rosakis, A. J., O. Samudrala, and D. Coker, 2000. Intersonic shear crack growth along weak planes. Mat. Res. Innovat., 3, pp. 236-243.

Rosakis, A. J., 2002. Intersonic shear cracks and fault ruptures. Advances in Physics, vol. 51, 1189-1257.

Rosakis, A.J., Xia, K.W., Lykotrafitis, G., Kanamori, H., 2007. Dynamic shear rupture in frictional interfaces : speeds, directionality and modes. In : Treatise in Geophysics, vol. 4. Elsevier, pp. 153-192.

Sanchez-Palencia, E., 1980. Non-homogeneous Media and Vibration Theory. Lecture Notes in Physics, vol.127, Springer, Berlin.

Schlüter, A., Kuhn, C., Müller, R., Gross, D., 2016. An investigation of intersonic fracture using a phase field model. Arch. Appl. Mech. vol. 86, 321-333.

Slepyan, L.I., 2002. Models and phenomena in fracture mechanics, Tel Aviv University.

Telega, J.J., 1990. Homogenization of fissured elastic solids in the presence of unilateral conditions and friction. Comput. Mech., 6, 109-127.

Wrzesniak A., Dascalu C., Besuelle P., 2014. A two-scale time-dependent model of damage : Influence of micro-cracks friction : European Journal of Mechanics A/Solids vol. 49, 345-361.

Zhao L.Y., Shao, J.F., Zhu, Q.Z., 2018. Analysis of localized cracking in quasi-brittle materials with a micro-mechanics based friction-damage approach, J. Mech. Phys. Solids, vol. 119, 163-187.

Zhu, Q.Z., Shao, J.F., 2015. A refined micromechanical damage-friction model with strength prediction for rock-like materials under compression. Int. J. Solids Struct. vol. 60, 75-83.

Zhu, Q.Z., Zhao, L.Y., Shao, J.F., 2016. Analytical and numerical analysis of frictional damage in quasi brittle materials. J. Mech. Phys. Solids, vol. 92, 137-163.